DALTON
FULL PAPER

Electronic structure and metal–metal bonding in nominal d^3 d^3 $M^{II}M^{IV}Cl_9^{3-}$ (M^{II} = V, Nb, Ta; M^{IV} = Mn, Tc, Re) face-shared binuclear complexes

Robert Stranger * and Simon Petrie

Department of Chemistry, the Faculties, the Australian National University, Canberra ACT 0200, Australia

Received 3rd May 2002, Accepted 26th June 2002
First published as an Advance Article on the web 12th August 2002

Density functional theory (DFT) calculations have been employed to study structural and electronic configuration trends in the series of mixed-group, face-shared, bimetallic complexes $M'M''Cl_9^{3-}$ (M' = V, Nb, Ta; M'' = Mn, Tc, Re), in which each metal possesses a nominal d^3 valence electronic configuration. While the tendency of complexes to exhibit either multiple metal–metal bonded structures (with short intermetallic separations) or weakly-coupled systems (characterized by large intermetallic distances) is broadly consistent with that seen in our earlier studies on same-group dimers (*e.g.* $Cr_2Cl_9^{3-}$), there are also several novel structural and electronic effects which are directly attributable to electron transfer from M^{II} to M^{IV}. The general tendency towards intermetallic electron transfer is well modelled by a simple expression involving the spin polarization energy of each metal, and the ligand-field splitting of t_{2g} and e_g orbitals, in the corresponding d^3-valence hexachloro octahedral complex. The effects of this electron transfer include, in some instances, a preference towards ferromagnetic coupling between metal atoms; diminished barriers to complex dissociation; and formation of edge-shared dimers with one five-coordinate metal atom. The heavier congeners, *i.e.* those lacking V and Mn, are predicted to have strong multiple metal–metal bonds with significant barriers to dissociation.

Introduction

While the nature of the metal–ligand bond is central to transition metal chemistry, the importance of interactions between adjacent metal atoms has also long been appreciated.[1] These intermetallic interactions range from strong, multiple metal–metal bonding to much weaker ferromagnetic or antiferromagnetic coupling between neighbouring metal atoms. One particularly valuable class of compounds, which has helped to forge an understanding of the interplay between d-orbital radii, metal ion electronic configuration, and bonding tendencies, is that of the face-shared nonahalides typified by $Cr_2Cl_9^{3-}$,[2–14] which are often referred to as 'dimers' of octahedral complexes and have a general structural formula $[X_3M'X_3M''X_3]^{n-}$. The flexibility of the ($M'X_3M''$) triply-bridged subunit[15] permits a wide range of intermetallic separations, so that both triple metal–metal bonded and weakly coupled bimetallic configurations can be accommodated without undue angle strain within the bridging moiety. A sizeable body of work, encompassing both experimental and theoretical investigations, now exists concerning the structural trends, particularly with respect to intermetallic interactions, evident among members of the set of face-shared dimers. The large majority of these previous studies have explored the bonding tendencies between metal atoms in homonuclear (*e.g.* $Cr_2Cl_9^{3-}$)[2] or same-group (*e.g.* $CrMoCl_9^{3-}$)[16] dimers, which show a very clear correlation between the metal atoms' d-orbital radii and the propensity for metal–metal bond formation *versus* weak antiferromagnetic coupling. Similar trends are also seen in a recent study[17] involving bimetallic complexes featuring metal atoms from neighbouring groups, as in $VCrCl_9^{4-}$ and $CrMnCl_9^{2-}$; amongst these compounds, electron transfer between metal atoms was found to have a significant structural impact, with several instances (invariably, those involving electron transfer to a first-transition-row atom) in which a ferromagnetically coupled complex was found to be the lowest-energy form.[17,18] One important motivation for the study of such complexes is the prospect of an improvement in our understanding of electron transfer effects in bioinorganic systems, for which several examples of heteronuclear combinations of transition metals (*e.g.* Cu^{II}/Fe^{III},[19,20] Ni^{II}/Fe^{III},[21] and Mn^{II}/Fe^{III})[22] are already known. An understanding of intermetallic electron transfer effects is also pertinent to our comprehension of bonding in homonuclear dimers such as $Cr_2Cl_9^{3-}$.[12–14,23] In the present study, we examine further the structural influence of electron transfer between metal atoms by studying a set of complexes, from $VMnCl_9^{3-}$ to $TaReCl_9^{3-}$, for which the disparity between oxidation states on the neighbouring metal atoms (assuming a d^3d^3 configuration) is more severe than that in any of our earlier studies.

As in previous studies, we have employed the broken-symmetry (BS) technique in density functional theory (DFT) calculations on the bimetallic complexes of interest. The broken-symmetry approach, which introduces an initial electron spin inhomogeneity between the two metal atoms, permits direct interconversion between weakly antiferromagnetically coupled and fully metal–metal bonded forms. The BS technique is therefore very valuable for determining the relative energies of weakly-coupled and strongly-bonded structures of a given complex, although an awareness of its limitations (for even-electron systems, it is strictly applicable only to configurations having $M_S = 0$) is also necessary. In previous studies, we have found that the BS potential energy curve may not always describe the lowest-energy structure in d^1d^1 (*e.g.* $Ti_2Cl_9^{3-}$)[24] or d^5d^5 (*e.g.* $Ru_2Cl_9^{3-}$)[25] homonuclear dimers, or in mixed-group d^3d^3 dimers (*e.g.* $NbCrCl_9^{4-}$):[17] the first two cases represent complexes in which incomplete occupation of either the 'bonding' (in d^1d^1 dimers) or the 'antibonding' subset (in d^5d^5 dimers) of the t_{2g}-derived orbitals may favour spin-triplet configurations, while amongst the mixed-group d^3d^3 dimers ferromagnetic coupling is favoured as a result of intermetallic electron transfer when the more highly oxidized transition metal atom is first-row.[17,18]

 DOI: 10.1039/b204303c

Computational details

All calculations described in this work were performed on Linux-based Pentium III 600 MHz computers using the Amsterdam Density Functional (ADF) program, version ADF2000,[26] developed by Baerends *et al.*[27] All calculations employed the local density approximation (LDA) to the exchange potential,[28] and the correlation potential of Vosko, Wilk, and Nusair.[29] Previous studies on a variety of dinuclear and polynuclear transition-metal-containing complexes[30–33] have shown that the LDA generally offers significantly better agreement with experimental geometries, particularly with regard to metal–metal distances, than do more computationally demanding DFT calculations incorporating nonlocal corrections to the exchange potential. The (possibly fortuitous) tendency of LDA to outperform existing gradient-corrected DFT methods is contrary to LDA's widely-acknowledged tendency to overbind,[34] but the good performance of LDA is further borne out in a recent detailed study specifically comparing the optimization of metal–metal bond lengths for a diverse 'test set' of dinuclear complexes, studied using various local and nonlocal functionals.[35] We have also chosen not to adopt the approach, frequently implemented by other groups, of using LDA-optimized geometries in single-point calculations using gradient-corrected methods. Our experience in this regard has been that single-point gradient-corrected calculations unrealistically favour nonbonded metal–metal interactions,[18] thus severely skewing the relationship between, for example, the $S = 0$ and $S = 3$ associated states which represent respectively strongly bonded and weakly coupled intermetallic interactions (see below). Even in calculations on ferromagnetic ($S = 3$) *versus* antiferromagnetic (BS) weakly-coupled configurations, gradient-corrected calculations appear prone to incorrectly predict the sign of the magnetic coupling constant J, as we have found[18] for the $CrMoCl_9^{3-}$ dimer which is known from experiment to exhibit moderate antiferromagnetic coupling,[16,36] in agreement with LDA calculations but contrary to the results of calculations using the popular gradient-corrected method B-LYP (either with LDA-optimized, or with B-LYP-optimized geometries).[18]

Basis sets for all atoms were the 'Type IV' bases of triple-ζ quality with Slater type orbitals. Electrons in orbitals up to and including 2p {Cl}, 3p {V, Mn}, 4p {Nb, Tc}, and 4f (but excluding 5s and 5p) {Ta, Re} were considered to comprise the core and were treated in accordance with the frozen-core approximation. Optimized geometries were obtained using the gradient algorithm of Versluis and Ziegler.[37] Full-symmetry calculations for the $S = 0$, $S = 2$, and $S = 3$ associated states and 'reference state' calculations of the type described previously,[38] and broken-symmetry calculations for the $S = 0$ state (employing an asymmetry in the initial spin densities upon the two metal atoms)[39] were performed in a spin-unrestricted manner using C_{3v} symmetry unless otherwise indicated. Potential energy curves for all pertinent states were obtained by optimization of all other structural parameters for the dimers along a series of fixed metal–metal separations.

The $S = 0$, $S = 2$, and $S = 3$ associated states afford descriptions of the bimetallic complex possessing, respectively, a triple metal–metal bond, a single metal–metal bond, or a weakly coupled, nonbonded interaction between metals. In our previous experience with d^3d^3 face-shared dimers,[15,17,18,24,25,30,38,40–42] one or other such associated state has always been found to correspond closely to the lowest-energy configuration of the dimer, and this experience is borne out also by the present results. Since it appears that, in C_{3v} symmetry, all of the complexes within the present study can satisfactorily be described as either antiferromagnetically coupled dimers for which the broken-symmetry approach works very well, or ferromagnetically coupled complexes for which the $S = 3$ associated state offers a good treatment, we have chosen not to pursue the nontrivial task of elucidating true relative energies for the various multiple-determinant species which, while chemically interesting, appear of negligible structural relevance to the set of complexes investigated here.

Results and discussion

Intermetallic bonding and electron transfer: a brief overview

The valence-d orbital diagram for a heteronuclear face-shared dimer $M_2X_9^{n-}$, shown in Fig. 1, illustrates the lowest-energy electronic configurations expected (within the 'broken-symmetry' constraint of $M_S = 0$, and with C_{3v} symmetry) for both the nonbonded and triply-bonded limiting cases. The t_{2g} orbitals of each 'monomeric' octahedral complex are, in the dimer, split into symmetry-distinct subsets (depending upon their orientation relative to the intermetallic axis) of a_1 (σ) and e (δ_π) symmetry. The minima for the various $S = 0$, $S = 2$, and $S = 3$ associated states correspond to, respectively, formal triple bond formation ($\sigma^2\delta_\pi^4$) with all valence-d electrons delocalized between the two metals; single bond formation with the remaining four electrons localized (and spin-aligned) within the t_{2g}-derived e orbital manifold; and localization of all six, spin-aligned, valence-d electrons within the a_1 and e orbitals in a weakly coupled complex. These orbital occupations, as well as that for the hypothetical 'reference state' which we have used to compare the stabilization due to orbital overlap and to spin polarization effects, are summarized in Fig. 2. In a well-behaved dimer, the minima on the $S = 0$, $S = 2$, and $S = 3$ associated state surfaces are found at progressively increasing intermetallic separations, in accordance with expectations based upon the extent of bonding as described above.

The energy level diagram (Fig. 1) expected for a heteronuclear dimer differs from that for a homonuclear dimer, due to the disparity in orbital energies for the two metal atoms. This orbital inequality influences the electronic structure of mixed-group dimers, as is apparent for the families of V/Cr and Cr/Mn mixed-group dimers which we have studied previously,[17] owing to significant electron transfer from the less-oxidized to the more-highly-oxidized metal atom. Within the V/Mn mixed-group dimers studied here such an effect (of distortion from a balanced d^3d^3 electronic configuration) is expected to be severe. Based on our findings for the V/Cr and Cr/Mn mixed-group dimers, we can envisage that (a) the occupied valence metal orbitals will in general have a much greater degree of character due to M″, the more highly oxidized metal, than due to M′, the less highly oxidized metal, and that (b) formal electron transfer from M′ to M″ may result in occupation of the β-spin t_{2g}-derived orbitals and/or of the e_g-derived orbitals on M″ depending on the ligand field splitting and spin polarization splitting on this metal. As a rule, electron transfer will operate against strong intermetallic bond formation (although this was not a notable consequence in our previous study of the V/Cr and Cr/Mn mixed-group dimers),[17] while it has the capacity to strengthen the spin polarization stabilization of the high-spin state (which, in our earlier study, was clearly evident for $M'CrCl_9^{4-}$ and $M'MnCl_9^{2-}$ dimers).[17]

General structural and energetic results

In Table 1, we present calculated metal–metal bond distances obtained for the minima of the $S = 0$, $S = 2$, and $S = 3$ associated states as well as their energies relative to that of the broken-symmetry minimum for each dimer. Optimized geometries of the broken-symmetry minima, which (for the exception of complexes exhibiting a preference for ferromagnetic coupling) are expected to correspond closely to the true lowest-energy structures for these species, are shown in Table 2. Calculated metal-atom spin densities, for the broken-symmetry minima and for the $S = 2$ and $S = 3$ associated state minima, are given in Table 3: these spin densities have been corrected for metal–

Table 1 Energetic and structural parameters determined for the minima of the $S = 0$, $S = 2$, and $S = 3$ associated states, and relative energies of the reference state and broken symmetry minimum for each dimer system

M′M″ [a]	$E_{rel}(S=0)$ [b]	r_0(M′–M″) [c]	$E_{rel}(S=2)$ [b]	r_2(M′–M″) [c]	$E_{rel}(S=3)$ [b]	r_3(M′–M″) [c]	E_{rel}(ref) [b,e]	E_{tot}(BS) [d,e]
VMn	0.952	2.382	−0.303	3.435	−0.540	3.355	3.062	−48.005
VTc	0.101	2.331	0.248	2.981	0.901	3.392	3.237	−49.255
VRe	0.131	2.398	0.260	2.941	1.133	3.396	3.376	−50.223
NbMn	0.013	2.404	−0.948	3.703	−0.986	3.646	2.799	−48.999 [f]
NbTc	0	2.408	1.323	3.081	1.955	3.597	4.101	−51.205
NbRe	0	2.484	1.259	3.049	2.379	3.545	4.244	−52.047
TaMn	0.002	2.456	−1.051	3.740	−1.073	3.726	2.889	−49.915
TaTc	0	2.494	1.426	3.088	1.928	3.700	4.180	−52.029
TaRe	0	2.506	1.562	3.066	2.622	3.595	4.510	−52.964

Notes: [a] Identity of the two metal atoms M′ and M″ in the bioctahedral complex $M'M''Cl_9^{3-}$. [b] Relative energy of the indicated state, $E_{tot} - E_{tot}$(BS), in electronvolts. [c] Optimized intermetallic separation for the $S = 0$, $S = 2$, or $S = 3$ state, in Å. [d] Total bond energy, E_{tot} of the broken-symmetry optimized geometry, in electronvolts. [e] Intermetallic separations for the reference state are very similar to those found for the $S = 3$ associated state; the intermetallic separations for the broken symmetry minima are detailed in Table 2. [f] For this species, two local minima are obtained on the broken symmetry potential energy surface. Minimum (1), the lower-energy species, has a geometry similar to that of the $S = 0$ associated state minimum, while minimum (2) has a geometry characteristic of a $S = 2$ associated state and an energy $E_{rel} = 0.092$ eV.

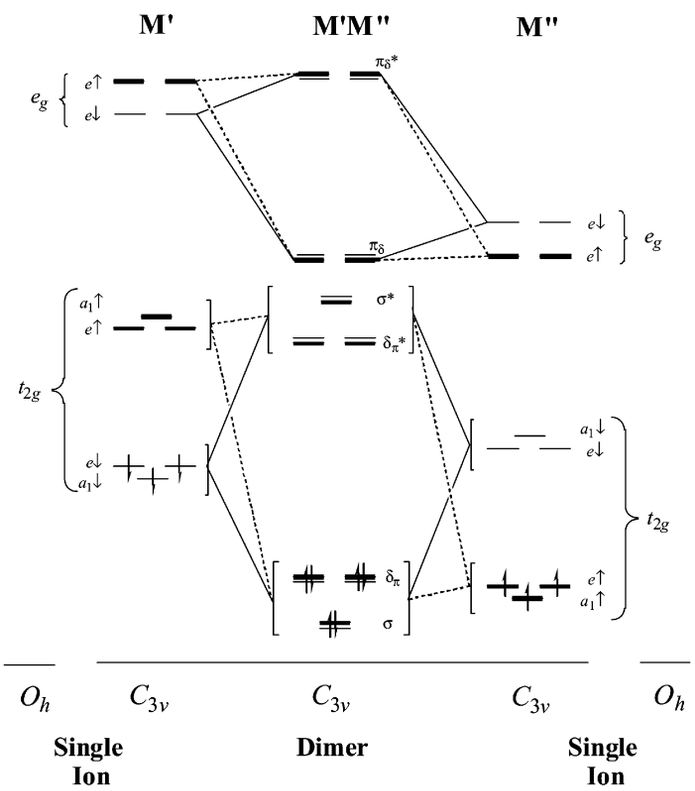

Fig. 1 Representation of the $S = 0$ broken-symmetry state of a mixed-group dimer $M'M''Cl_9^{n-}$, in both localized and delocalized limits. Orbitals are labelled according to the representations of the C_{3v} point group.

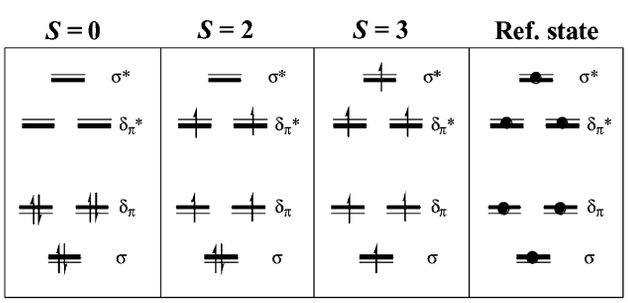

Fig. 2 Representation of t_{2g}-derived orbital occupancy for the $S = 0$, $S = 2$, and $S = 3$ associated states, and for the reference state, for a generic dimer $M'M''Cl_9^{n-}$.

ligand bond covalency effects by the scale factor $3/\rho_{M(oct)}$, where $\rho_{M(oct)}$ is the Mulliken spin density of the central metal atom within the isolated high-spin d^3 octahedral complex MCl_6^{n-}. A justification for the use of this scaling procedure, which is designed to aid interpretation of the metal atom spin densities with respect to occurrence of metal–metal bonding and/or intermetallic electron transfer, has been presented in our previous study on the V/Cr and Cr/Mn mixed-group dimers.[17]

M′MnCl$_9^{3-}$ (M′ = V, Nb, Ta)

When C_{3v} symmetry is imposed, the $M'MnCl_9^{3-}$ dimers possess the following noteworthy points of divergence from the trends seen for same-group d^3d^3 dimers:

(i) The $S = 3$ associated state minimum is consistently at a substantially lower energy than the broken-symmetry ($M_S = 0$) minimum.

(ii) The $S = 2$ associated state minimum is also lower in energy than the BS minimum, and above $S = 3$ (but for M′ = Nb and Ta the gap between $S = 2$ and $S = 3$ is very small, < 0.05 eV).

(iii) For all three species, the M′–M″ distance obtained for the

Table 2 Optimized geometries of the broken-symmetry minima $M'M''Cl_9^{3-}$. Bond lengths are in Å and bond angles are in degrees

M′M″	$r_{Cl-M'}$ [a]	$\angle_{ClM'M''}$ [a]	$r_{M'-M''}$	r_{Cl-X} [b]	$\angle_{ClXM'}$ [b]	$\angle_{M'M''Cl}$ [a]	$r_{M''-Cl}$ [a]
VMn	2.375	123.0	3.092	1.812	92.8	124.6	2.299
VTc	2.377	124.7	2.620	2.051	89.7	124.9	2.418
VRe	2.375	124.4	2.615	2.068	90.0	125.0	2.428
NbMn	2.502	124.0	3.112	1.863	94.1	124.7	2.306
NbTc	2.499	124.9	2.407	2.212	90.3	123.2	2.416
NbRe	2.496	124.5	2.484	2.205	90.8	123.5	2.425
TaMn	2.501	125.8	2.487	2.084	91.6	124.3	2.318
TaTc	2.491	125.5	2.494	2.187	89.5	122.8	2.416
TaRe	2.492	124.9	2.507	2.193	90.1	123.2	2.428

Notes: [a] Terminal Cl atom in dimer. [b] Bridging Cl atom in dimer. The position of the bridging Cl ligands is defined relative to the midpoint, 'X', of the M′–M″ bond.

Table 3 Mulliken spin densities determined for the $S = 2$, $S = 3$, and broken-symmetry minima of the mixed-group dimers, adjusted for metal–ligand bond covalency

	$S = 2$		$S = 3$		BS		MCl_6^{n-}	
M′M″	$\rho_{spin}(M')$	$\rho_{spin}(M'')$	$\rho_{spin}(M')$	$\rho_{spin}(M'')$	$\rho_{spin}(M')$	$\rho_{spin}(M'')$	$\rho_{spin}(M')$	$\rho_{spin}(M'')$
VMn	−0.72	4.57	1.63	4.27	2.11	−2.23	3.15	2.90
VTc	1.99	2.09	2.26	3.93	1.63	−1.89	3.15	2.30
VRe	2.03	2.00	2.56	3.46	1.62	−1.85	3.15	2.26
NbMn	−0.84	4.81	1.00	4.77	1.67	−1.87	3.06	2.90
NbTc	1.63	2.45	1.52	4.8	0	0	3.06	2.30
NbRe	1.82	2.18	1.98	4.15	0	0	3.06	2.26
TaMn	−0.85	4.83	0.93	4.83	0.46	−0.63	3.04	2.90
TaTc	1.31	2.84	1.21	5.24	0	0	3.04	2.30
TaRe	1.71	2.32	1.65	4.62	0	0	3.04	2.26

Notes: [a] Covalency-corrected values. The method of covalency correction is described within the text. [b] Spin densities for the octahedral complexes; these values are not covalency-corrected. [c] Results for BS(2). For BS(1), values of −1.93(Ta) and +2.12(Cr) are obtained.

$S = 2$ minimum is unexpectedly larger than the corresponding distance for the $S = 3$ minimum (recall that $S = 2$ is generally expected to correspond to a complex featuring a metal–metal σ bond, while $S = 3$ corresponds to the weakly coupled case).

Features (i) and (ii) are entirely consistent with the structural and energetic tendencies of the V/Cr and Cr/Mn mixed-group dimers,[17] when M″ is first-row, while (iii), the lengthening of the $S = 2$ minimum relative to $S = 3$, can be considered as an exaggerated continuation of a trend towards longbonded $S = 2$ structures also evident in the $M'CrCl_9^{4-}$ and $M'MnCl_9^{2-}$ dimers.[17] None of these features are seen in any of the same-group d^3d^3 dimers, and we have previously attributed this distinction between same-group and mixed-group dimers as arising from significant intermetallic electron transfer towards M″, favoured for $S = 2$ and $S = 3$ by the large spin polarization stabilization energy of first-row M″.[17]

Orbital energy level diagrams, for the various V/Mn associated state and broken-symmetry minima, are shown in Fig. 3. For $S = 0$, the t_{2g}-based orbitals correspond to bonding and antibonding σ and δ_π molecular orbitals (MOs); it is apparent that the occupied bonding MOs contain a predominance of Mn character over V (while the vacant antibonding orbitals have considerable V content). The e_g-derived orbitals on the two metals can be treated as essentially pure atomic orbitals (AOs), since there is very little mixing evident between them. Thus the $S = 0$ associated state does represent a triply bonded structure (as expected), but a highly polar one.

The $S = 2$ and $S = 3$ associated states are electronically similar to each other, as is consistent with their close structural similarity, with the a_1 MOs corresponding very closely to the d_{z^2} AO on Mn or on V. There is a similar lack of mixing in the occupied α-spin 13e MO pair, which show only Mn δ_π content. The only occupied MOs to show mixing, in each of $S = 2$ and $S = 3$, are the α-spin 14e pair: these represent a blend between V δ_π and Mn e_g character, but (in contrast to the situation observed for the various V/Cr and Cr/Mn mixed dimers) [17] the Mn e_g content predominates. Clearly (since each of these associated states shows Mn in sole possession of three valence electrons and with a majority stake in two more) the $S = 2$ and $S = 3$ structures cannot be considered as d^3d^3 configurations: they correspond more properly to d^2d^4 or even d^1d^5 species, as indicated by the spin densities recorded for each metal atom (see Table 3). The effect of V ⟶ Mn electron transfer, on the relative spin polarization splittings of the two metal atoms (which in the d^3 octahedral complexes are broadly comparable) is also evident in these energy level diagrams.

The broken-symmetry minimum-energy configuration shows V ⟶ Mn electron transfer to a similar extent to that seen in $S = 2$ and $S = 3$; but transfer of β-spin electron density to Mn cannot enhance the spin-polarization stabilization of Mn's α-spin orbitals in the manner seen for α-spin electron transfer in $S = 2$ and $S = 3$, and consequently the BS configuration is considerably higher in energy. The magnitude of V ⟶ Mn electron transfer in these systems, and the varying impact of α- or β-spin transfer on the Mn spin-polarization splitting, can be appreciated on comparing the α-spin 14e (Mn e_g-derived MO)/β-spin 14e (Mn t_{2g}-derived MO) energy splitting for $S = 3$ and for BS: for $S = 3$, these two levels are separated by 1.77 eV, while for BS these MOs are virtually degenerate.

Since the energetic benefits of electron transfer are most pronounced for the $S = 2$ and $S = 3$ associated states, it is reasonable to suppose that it is these associated states which show the greatest extent of V ⟶ Mn electron transfer. A comparison of the bar charts for MO composition in the various electronic configurations, in Fig. 3, broadly supports this view. We might also expect that the calculated atomic charges on V and on Mn would show such a phenomenon, but this is not so: the lowest Mulliken charges on Mn are seen for the $S = 0$ and BS configurations, apparently indicating a *larger* extent of electron transfer to Mn for $S = 0$ and BS than for $S = 2$ or $S = 3$. Interpretation of the Mulliken data is problematic, since population of the Mn α-spin e_g orbitals (as occurs with α-spin V ⟶ Mn electron transfer in $S = 2$ and $S = 3$) results in a much greater extent of charge donation to the surrounding Cl atoms than occurs with

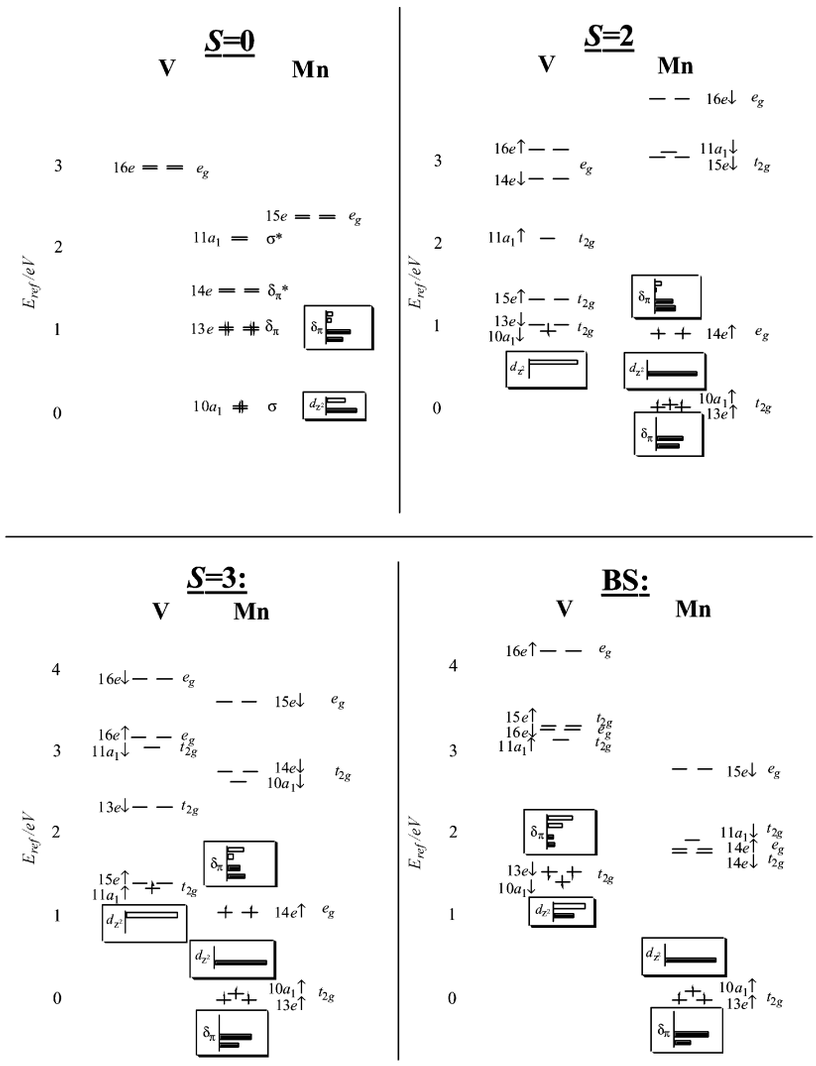

Fig. 3 Electronic configurations of the associated state ($S = 0$, $S = 2$, $S = 3$) and broken symmetry minima of $VMnCl_9^{3-}$. In this and subsequent electronic configuration diagrams relating to C_{3v}-symmetry structures, the molecular orbitals shown, which are labelled according to their hierarchy (excluding 'frozen core' orbitals), are those identified as arising principally from the valence-d atomic orbitals of the metal atoms. Metal AO contributions to the occupied molecular orbitals are shown as overlaid bar charts, with M′ shown as outlined (white) bars and M″ as filled (black) bars; for a_1- or σ-symmetry MOs, only d_{z^2} content is shown, while for e-symmetry orbitals, the two bars depicted for each metal are: upper bar, $d_{x^2-y^2}$ (or d_{xy}) content; lower bar, d_{xz} (or d_{yz}) content.

V ⟶ Mn β-spin transfer, and it appears that this phenomenon obscures our view of the intermetallic interaction.

The polarization of the M′–Mn axis is even more extreme for the heavier V-group metals. If we examine the valence metal MO composition of the C_{3v} $S = 3$ and broken-symmetry structures of $TaMnCl_9^{3-}$ (see Fig. 4), we find that the electronic configuration conforms very closely to d^1d^5, with very little mixing between the metals (consistent with the very large Ta–Mn separation of 3.7 Å) and with only the occupied α-spin $13a_1$ orbital localized on tantalum. Another curiosity of the $S = 3$ orbital energy level diagram is the reversal of relative energies for the Mn α-spin t_{2g}-based (δ_π) and e_g-based π_δ) orbitals: this is a consequence of the $S = 3$ C_{3v} structure, which is quite markedly distorted away from a bioctahedral shape towards a $[Ta^{IV}Cl_6^{2-}\cdot Mn^{II}Cl_3^{-}]$ geometry. The trend towards planarity of the $MnCl_3^-$ moiety, in the $S = 3$ C_{3v} structure, is not total: the ∠(ClMnTa) value of 113.8° is only about 10° smaller than a typical homonuclear dimer value, but this change in the coordination environment is evidently sufficient to invert the δ_π and π_δ orbitals. The adoption of a d^1d^5 electronic configuration, which is of course a consequence of the very substantial imbalance between the Ta^{II} and Mn^{IV} valence orbital energies (coupled with the preference of Mn for a high-spin configuration), also helps to account for the extraordinarily large intermetallic separation seen for the $S = 2$ geometry (and similarly for $NbMnCl_9^{3-}$): the $S = 3$ and $S = 2$ configurations effectively differ solely in the alignment, or opposition, of the sole Ta valence electron with the high-spin Mn^{II} centre. The Mn^{II} oxidation state in these species is stabilized by exclusively α-spin population of the Mn valence orbitals, and this avenue is blocked in the broken-symmetry state in which the α and β electron counts are equal. A point of interest here is that, while the Ta–Mn bond (2.487 Å) in the BS state is elongated only very marginally from that of the triply-bonded $S = 0$ minimum (2.456 Å), the spin densities on Ta and Mn (−0.46 and 0.63, respectively) cannot be dismissed as negligible: evidently the drive towards spin polarization on Mn is strong, even at short Ta–Mn separations. The spin-asymmetry of the BS minimum appears to result from the small energy separation between the $S = 0$ minimum and the $S = 2$ surface at this intermetallic separation.

It is worth reiterating that the broken-symmetry minima for all of the $M'MnCl_9^{3-}$ dimers are structurally and/or energetically far removed from the apparent global minima for these species, which show a very strong preference for high-spin d^5 Mn configurations. It is, indeed, relevant to query whether these d^1d^5 dimers have any real (kinetic or thermodynamic) stability against dissociation to separated $M'Cl_6^{2-}$ and $MnCl_3^-$

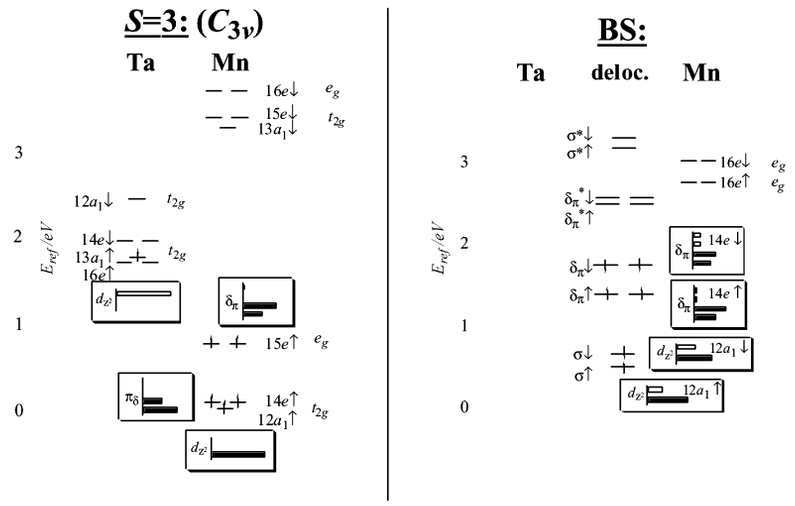

Fig. 4 Electronic configuration of the $S = 3$ and broken symmetry structures of $TaMnCl_9^{3-}$, optimized in C_{3v} symmetry. See Fig. 3 for an explanation of the orbital content bar charts.

moieties. Linear transit calculations performed in C_{3v} symmetry, in which the M′–Mn bond is systematically increased while other parameters are optimized, indicate that the barrier to separation is more substantial for $VMnCl_9^{3-}$ (barrier height = 0.50 eV for $S = 3$) than for $NbMnCl_9^{3-}$ or $TaMnCl_9^{3-}$ (with barrier heights of 0.12 and 0.09 eV, respectively, for C_{3v}-symmetric dissociation of the $S = 3$ associated state).

We have also perfomed optimizations of the $S = 3$ associated state species in C_s symmetry: in these calculations, the structure obtained for $VMnCl_9^{3-}$ is identical to that found when C_{3v} symmetry is imposed (indicating that the face-shared geometry is the preferred configuration for this species) but the $NbMnCl_9^{3-}$ and $TaMnCl_9^{3-}$ dimers spontaneously distort away from a face-shared geometry to an edge-shared structure (in which Nb or Ta obtains sole custody of a formerly bridged Cl). These edge-shared species appear not to be well described by a single-determinant wavefunction, since all feasible initial discrete-electron orbital occupations investigated resulted in non-Aufbau electronic configurations (resulting, principally, from the near-degeneracy of the α-spin t_{2g}-based orbitals on d^1 Nb or Ta). Marginally lower total energies were obtainable for occupations in which the single valence electron on Nb or Ta was distributed across two or three of the α-spin t_{2g}-derived orbitals, supporting the inference that a multi-determinant wavefunction is required to properly describe these species. Allocation of the Nb or Ta valence electron within the α-spin t_{2g}-derived orbital manifold had negligible impact on the structure obtained through optimization. In the discussion which follows, we shall focus on the lowest-energy discrete electron occupation for the C_s symmetry $S = 3$ dimer.

The $S = 3$ $NbMnCl_9^{3-}$ and $TaMnCl_9^{3-}$ edge-shared structures are slightly lower in energy than their face-shared counterparts (by 0.12 and 0.14 eV, respectively, for M′ = Nb and Ta) but still possess insubstantial barriers to dissociation (with barrier heights of 0.11 and 0.09 eV, respectively). Due to the appreciable $M'Cl_6^{2-} \leftrightarrow MnCl_3^-$ Coulombic repulsion term which still exists at the dissociation barrier (at an intermetallic separation of 4.5–5 Å, the Coulombic repulsion between a dianion and a monoanion is in the range 5.9–6.5 eV if the charges are considered to be centred on the metal atoms), none of the (gas-phase) $M'MnCl_9^{3-}$ structures are thermodymanically stable with respect to the separated $M'Cl_6^{2-}$ and $MnCl_3^-$ products. The situation within solution, or in a crystalline environment, may well be very different due to the stabilizing influence of solvation or of surrounding counterions, so the apparent fragility of these species in the gas phase does not necessarily indicate poor prospects for the experimental isolation of some examples of these weakly-coupled dimers.

$VM''Cl_9^{3-}$ (M″ = Tc, Re)

These compounds are 'well-behaved' in the sense that the broken-symmetry state comprises the lowest-energy structure, which in each case possesses a M′–M″ distance roughly intermediate between those of the $S = 0$ and $S = 2$ associated states. Such a result is consistent with the comparatively slight gap (0.13–0.15 eV) between the $S = 0$ and $S = 2$ minima. In contrast to the $M'MnCl_9^{3-}$ species described above, the $VM''Cl_9^{3-}$ $S = 0$, $S = 2$, and $S = 3$ associated state structures all differ distinctly in their M′–M″ bond lengths; these intermetallic distances also follow the expected trend with $r_{(S=0)} < r_{(S=2)} < r_{(S=3)}$, suggesting (again in contrast to the $M'MnCl_9^{3-}$ species) that the $S = 2$ configurations for $VTcCl_9^{3-}$ and $VReCl_9^{3-}$ possess significant M′–M″ σ-bonding character. The $S = 2$ and $S = 3$ minima are also widely spaced energetically, with a gap exceeding 0.6 eV in each case.

Analysis of the broken-symmetry MO composition (see Fig. 5), for the example of $VReCl_9^{3-}$, suggests a structure characterized by V–Re σ bond formation with little additional δ_π bonding: the α-spin δ_π MO is localized on Re, while the β-spin δ_π MO shows a comparatively limited extent of electron transfer 'leakage' from V to Re. The σ-bonding MOs show a much greater degree of shared electron character, consistent with (polar) covalent bond formation. For both the σ- and δ_π-symmetry occupied MOs, there is a tendency for net electron donation towards Re (as a consequence of the V/Re orbital energy gap) and also for β-spin electron retention by V (which favours spin-polarization stabilization of the V-based MOs).

The "Lewis acid" metal atom M″ in these systems (*i.e.*, Tc or Re) is one more strongly influenced by ligand-field splitting than by spin polarization stabilization, while the reverse is true of the "Lewis base" metal, V. It follows that the occurrence of V ⟶ M″ α-spin electron transfer for the $S = 3$ associated state will diminish the total (V + M″) spin polarization stabilization energy for the complex, and that therefore V ⟶ M″ electron transfer will be disfavoured. This supposition is borne out by the $S = 3$ energy level diagram for $VReCl_9^{3-}$ in Fig 5. The occupied α-spin $12a_1$ and 14e MOs are localized purely on Re, $13a_1$ is localized on V, and 15e exhibits only a small degree of contamination by Re in an essentially V-based MO. In consequence, the $S = 3$ configuration for $VReCl_9^{3-}$ approximates more closely than any other of the mixed-group dimer structures studied here to a 'pure' d^3d^3 valence electron configuration: from the corrected spin densities in Table 3, we obtain a configuration of $\sim d^{2.6}d^{3.4}$ for $VReCl_9^{3-}$ (and $\sim d^{2.2}d^{3.8}$ for $VTcCl_9^{3-}$). The modest distortion from d^3d^3 for $VReCl_9^{3-}$ contrasts with the d^1d^5 configuration attained for $S = 3$ $TaMnCl_9^{3-}$.

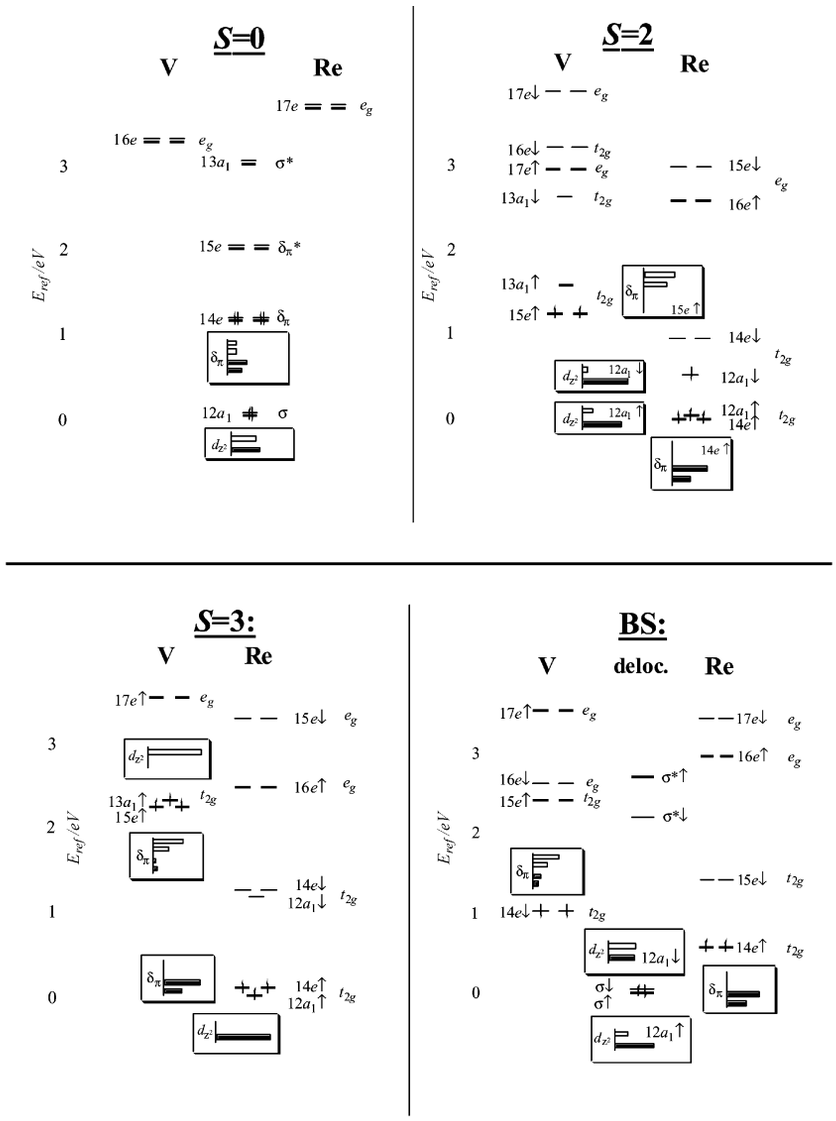

Fig. 5 Electronic configuration of the associated state and broken symmetry structures of $VReCl_9^{3-}$. See Fig. 3 for an explanation of the orbital content bar charts.

The optimized structures for the $S = 2$ associated state minima suggest the presence of a metal–metal single bond, and the corrected spin densities for these species (see Table 3) are very close to the values of +2 for each metal atom expected for a 'classical' $S = 2$ structure featuring an equally-shared σ-bond and two localized α-spin δ_π electrons on each metal. However, the MO contributions (detailed in Fig. 5 for the example of $VReCl_9^{3-}$) show that the V–M″ bond is highly polar, with a large excess of Re character over V for both the α- and β-spin components. This contrasts with the orbital content for the triply-bonded $S = 0$ configuration, in which the σ-bond is much more covalent in character (and where V ⟶ Re electron transfer is chiefly effected through polarization of the δ_π bonding orbitals).

The single common feature of all of the $VReCl_9^{3-}$ electronic configurations (true, by analogy, also for $VTcCl_9^{3-}$) is that they exhibit a significant extent of V ⟶ Re electron transfer, as is consistent with the relative energies of the V^{II} and Re^{IV} valence d-orbital manifolds. That the dominant mode of electron transfer differs for each of the $S = 0$, $S = 2$, $S = 3$ and broken-symmetry configurations serves to emphasize the influence of spin polarization splitting and ligand field splitting on the optimal electron distribution, in regard to both the mode of metal/metal interaction (whether weakly coupled or strongly bonded) and the polarization of the metal–metal axis.

Laboratory isolation of the $VTcCl_9^{3-}$ and $VReCl_9^{3-}$ complexes may be feasible: according to our calculations, these complexes adopt structures in which the bridging chlorides appear reasonably firmly bonded to each metal atom, implying a significantly greater barrier to complex dissociation (in the gas phase) than is found for the $M'MnCl_9^{3-}$ species.

$M'M''Cl_9^{3-}$ (M′ = Nb, Ta; M″ = Tc, Re)

These complexes, which contain only second- or third-row transition metals, all exhibit formation of metal–metal triple bonds as characterized by the convergence of the broken symmetry results to the $S = 0$ associated state minima. Partially or completely localized configurations are very much disfavoured as diagnosed by the high relative energies for σ-bonded $S = 2$ and, higher still, for $S = 3$. M′ ⟶ M″ electron transfer still occurs, however, as can be appreciated from the examples of $S = 3$ and BS configurations for $TaReCl_9^{3-}$ (see Fig. 6). In both of these cases, which are representative of the complexes under this heading, a valence electron configuration between d^1d^5 and d^2d^4 (see also Table 3) offers the best description.

Evaluation of the intermetallic electron transfer is most straightforward for the $S = 3$ configuration (for which there is an obvious relationship between the extent of α-spin electron transfer and the observed metal atom spin densities), and we

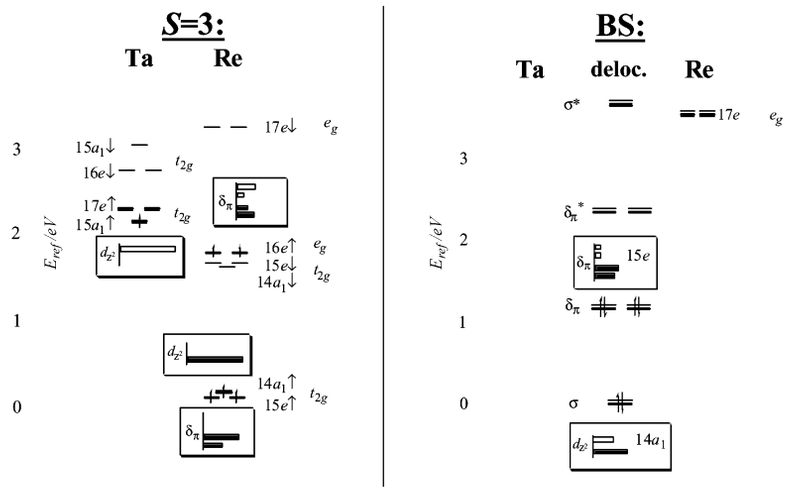

Fig. 6 Electronic configuration of the $S = 3$ and broken symmetry structures of $TaReCl_9^{3-}$. See Fig. 3 for an explanation of the orbital content bar charts.

note that the degree of electron transfer in the $S = 3$ $M'M''Cl_9^{3-}$ (M′ = Nb, Ta; M″ = Tc, Re) complexes is essentially intermediate between the $VM''Cl_9^{3-}$ (M″ = Tc, Re) and $M'MnCl_9^{3-}$ (M′ = Nb, Ta) configurations. We have previously reported an analogous trend (albeit smaller in magnitude) for the V/Cr and Cr/Mn mixed-group dimers.[17]

An illustration of the $S = 3$ associated state's electron transfer tendency is given in Fig. 7, for which the parameter arrayed on the ordinate axis, $\Delta(M'') - \delta(E_{SPE})$, is defined

$$\Delta(M'') - \delta(E_{SPE}) = \Delta(M''Cl_6^{2-}) + E_{SPE}(M'Cl_6^{4-}) - E_{SPE}(M''Cl_6^{2-}) \quad (1)$$

where Δ and E_{SPE} are respectively the ligand-field splitting and the spin-polarization stabilization energy of the octahedral complex indicated, Table 4. Occurrence of α-spin electron transfer is hampered by a large spin polarization stabilization energy for M′ (since electron transfer drains electron density from the stabilized α-spin orbitals on M′) and by a large ligand field splitting value for M″ (since α-spin transfer must result in population of the e_g-based orbitals: destabilization of these orbitals mitigates against electron transfer), while conversely a large spin polarization stabilization energy for M″ favours α-spin transfer. The dependence of α-spin electron transfer on the parameter $\Delta(M'') - \delta(E_{SPE})$ is quite evident, though it is not (nor would we expect it to be) a purely linear relationship: among other considerations, E_{SPE} does not scale linearly with

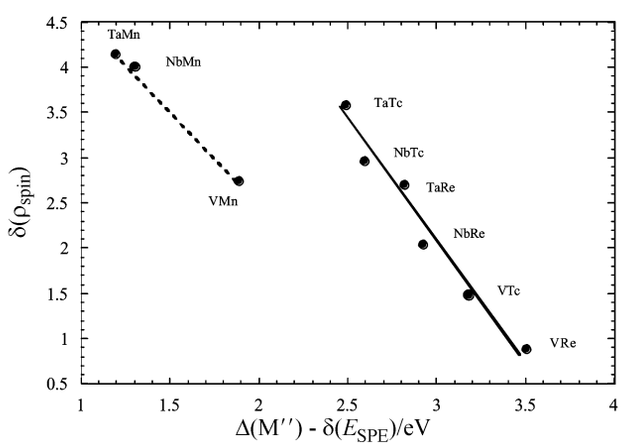

Fig. 7 This graph illustrates the dependence of the $S = 3$ associated state's intermetallic spin density asymmetry $\delta(\rho_{spin})$, where $\delta(\rho_{spin}) = 6 - 2\rho_{spin}(M')$, on the parameter $\Delta(M'') - \delta(E_{SPE})$. The solid and dotted lines are intended as visual aids, rather than as an accurate fit to the data obtained in the present work.

Table 4 Overlap and spin polarization stabilization energies determined for mixed-group dimers

M′M″	E_{ovlp} [a]	E_{SPE} [a]	$E_{SPE}(M')$ [b]	$E_{SPE}(M'')$ [b]	δ_{SPE} [c]
VMn	2.110	3.602	1.828	1.636	0.14
VTc	3.136	2.336	1.828	0.885	−0.38
VRe	3.245	2.243	1.828	0.791	−0.38
NbMn	2.786	3.785	1.244	1.636	0.91
NbTc	4.101	2.146	1.244	0.885	0.02
NbRe	4.244	1.865	1.244	0.791	−0.17
TaMn	2.887	3.962	1.137	1.636	1.19
TaTc	4.180	2.252	1.137	0.885	0.23
TaRe	4.510	1.888	1.137	0.791	−0.04

Notes: [a] Parameter, in eV and as defined in text, for the mixed dimer. [b] Spin polarization stabilization energy (in eV) for the octahedral complex containing the indicated metal ion. [c] $\delta_{SPE} = E_{SPE}(M'M'') - (E_{SPE}(M') + E_{SPE}(M''))$, expressed in eV.

metal-atom spin density; the e_g-based orbitals on M″ can accept at most two α-spin electrons, so that the capacity for electron transfer is quite limited; and the ligand field splitting associated with a distorted octahedral arrangement of ligands in a face-shared complex will differ from the pure octahedral value of a monomeric complex. The approximation to a linear dependence in Fig. 7 becomes much better if we distinguish between the complexes which favour ferromagnetic intermetallic coupling ($M'MnCl_9^{3-}$, dashed line) and those for which the lowest-energy configuration is low-spin ($M'TcCl_9^{3-}$ and $M'ReCl_9^{3-}$, solid line). The most plausible justification for this dichotomy within the $S = 3$ electron transfer results is that the $M'MnCl_9^{3-}$ dimers feature significant Mn e_g-based orbital occupation (and hence a larger degree of metal–ligand covalency), while the $M'TcCl_9^{3-}$ and $M'ReCl_9^{3-}$ dimers are essentially confined exclusively to t_{2g}-based orbital occupancy.

Comparison with same-group $M'M''Cl_9^{3-}$ dimers

The tendencies evident in our earlier comparison of mixed-group dimers (*viz.*, the V/Cr and Cr/Mn triad combinations)[17,18] with their same-group counterparts (*i.e.*, the dimers of the V,[42] Cr,[30,38,40] and Mn[30] triads) are upheld also in the present study on the V/Mn triad combinations. These tendencies can very satisfactorily be depicted in diagrammatic form as shown in Fig. 8, which shows the dependence of ferromagnetic *versus* antiferromagnetic coupling, and weak coupling *versus* significant metal–metal bonding, on the row numbers and group numbers of the constituent metal atoms M′ and M″. The factors which govern the preferred mode of intermetallic interaction in any given dimer have already received attention in our previous studies[17,18,30,38,40] as well as in the preceding

Table 5 A comparison between the lowest-energy dimers found for the weakly-coupled $M'M''Cl_9^{3-}$ species

Parameter	M′M″			
	CrCr	VMn	NbMn	TaMn
Overall charge state	3−	3−	3−	3−
Electronic configuration	d^3d^3	$\sim d^{1.5}d^{4.5}$	d^1d^5	d^1d^5
M′–M″ coupling	Antiferromagnetic	Ferromagnetic	Ferromagnetic	Ferromagnetic
M′–M″ distance/Å	3.17	3.35	4.19	4.22
M–Cl (terminal)/Å	2.33	2.35 (V) 2.36 (Mn)	2.46[a] (Nb) 2.37[a] (Mn)	2.46[a] (Ta) 2.36[a] (Mn)
M–Cl (bridging)/Å	2.41	2.38 (V) 2.57 (Mn)	2.47 (Nb) 2.78 (Mn)	2.46 (Ta) 2.80 (Mn)
Mode of ligand bridging	Face-shared	Face-shared	Edge-shared	Edge-shared
Dissociation barrier/eV	≥5.48	0.50	0.11	0.09
$D(M'Cl_6–M''Cl_3)^{3-}$/eV	5.48[b]	−3.59[c]	−3.88[c]	−3.89[c]
$D(M'Cl_3–M''Cl_6)^{3-}$/eV	5.48[b]	−1.72[d]	−0.26[d]	0.46[d]

Notes:[a] Average of non-identical values. [b] For dissociation to $CrCl_6^{3-}$ and $CrCl_3$. [c] Dissociation to $M'Cl_6^{2-}$ and $MnCl_3^-$. [d] Dissociation to $M'Cl_3^-$ and $MnCl_6^{2-}$.

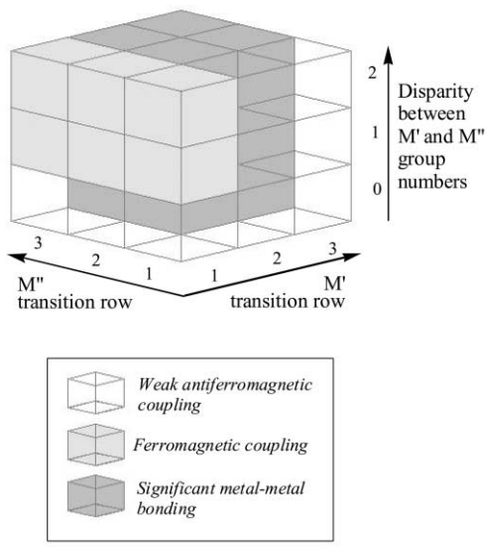

Fig. 8 A diagrammatic summation of metal–metal interaction tendencies in nominally d^3d^3 face-shared nonachloride dimers, expressed as a function of metal atom transition row number (where M′ is the less, and M″ the more highly oxidized d^3-valence metal atom) and of the difference in group number between M″ and M′. As specified in the legend, the shading indicates the preferred mode of metal–metal coupling according to our DFT calculations.

sections of this work, and need not be further elaborated here. Nevertheless, some comparisons between specific examples of mixed- and same-group dimers may prove informative.

Notwithstanding their apparent fragility as described in the preceding section, the $M'MnCl_9^{3-}$ complexes are still of interest as an 'extreme case' among the range of possible metal dimer structures. It is particularly pertinent to contrast the $VMnCl_9^{3-}$ dimer with its nominally isoelectronic counterpart $Cr_2Cl_9^{3-}$: both are species which exhibit a preference for weak coupling between the metal atoms rather than significant metal–metal bond formation, but the V/Mn dimer has a valence orbital energy level mismatch which the homonuclear chromium dimer lacks. Structural features of these complexes, and of the weakly-coupled $NbMnCl_9^{3-}$ and $TaMnCl_9^{3-}$ dimers, are summarized in Table 5. This M′/Mn orbital energy disparity drives the M′ ⟶ Mn electron transfer, which results in four key differences between the Cr/Cr and M′/Mn dimers:

(i) Most obviously, electron donation from M′ to Mn brings about a distortion of the electronic configuration, from d^3d^3 (as in the Cr/Cr 'norm') towards d^1d^5.

(ii) The disparity of valence d electron content (Mn has a clear excess over M′), and the preference of d^5 Mn for a high-spin electronic configuration, together effectively overturn the 'normal' preference for antiferromagnetic coupling between metal atoms (as seen in the weakly-coupled Cr/Cr dimer): the lowest-energy M′/Mn dimers are ferromagnetically coupled, since this configuration appears to offer the greatest opportunity for spin polarization stabilization of the d^5 Mn atom.

(iii) Population of e_g-type valence orbitals on Mn influences the Mn–Cl bonding, so that a pseudo-octahedral configuration around Mn is destabilized. The large disparity between 'bridging' and 'terminal' Cl–Mn bond lengths reflects the tendency towards $M'Cl_6^{2-}/MnCl_3^-$ dissociation, while the weakness of the bridging interactions with Mn (particularly for the edge-shared Nb/Mn and Ta/Mn complexes) is indicated by the low gas-phase barrier to dissociation.

(iv) The ultimate influence of electron transfer is to open up a new avenue for dimer fragmentation (to $M'Cl_6^{2-}$ and $MnCl_3^-$) in a manner not possible for $Cr_2Cl_9^{3-}$. As shown by the data in Table 5, there is a tremendous difference between the $D(M'Cl_6–M''Cl_3)^{3-}$ values (which represent the bond strengths against formation of infinitely separated products) of the Cr/Cr and M′/Mn weakly-coupled dimer trianions, with a decrease by ~9 eV in the thermodynamic stability against dissociation of the M/Mn dimers relative to that for Cr/Cr. This massive thermodynamic effect is a direct result of the large Coulombic repulsion between incipient fragments in the lowest-energy M/Mn dimers, a mode of repulsion which is totally lacking in the $CrCl_6^{3-}$ and $CrCl_3$ fragmentation pathway of the Cr/Cr dimer. Of course, this effect applies strictly to dimers within the vacuum phase, for which the gas phase remains a reasonably close analogue: in solution or in the solid state, solvent effects and/or counterions will have a major structural influence. Our calculations do not, also, consider the reactivity of the metal dimers towards other solution-phase species, or towards disproportionation processes. Nevertheless, it seems pertinent to regard the chromium(III) ion as being particularly well fitted for weakly-coupled nonachloride dimer formation because of its charge state; this raises the possibility that, while the 'nominally d^3d^3' $M'MnCl_9^{3-}$ dimers may not ultimately prove isolable within the laboratory, other 'd^3d^3' M′Mn architectures (with different bridging and terminal ligands, deployed so as to minimize Coulombic destabilization of the metal–metal interaction) may well be less susceptible to fragmentation.

An analogous comparison, between same-group and mixed-group examples of 'd^3d^3' trianionic dimers with apparent triple metal–metal bonds, is also informative (see Table 6). For these species also we find that the thermodynamic stability of the same-group dimers (MoMo, MoW, and WW) is much greater than their mixed-group counterparts, but there is nothing like the structural diversity seen for the weakly interacting complexes. It is, of course, reasonable to expect a rather greater degree of structural robustness for species with a central multiple bond (augmented by significant Cl-bridging interactions with both metals) than for species lacking any significant metal–metal interaction, and this may well reflect better prospects for the laboratory isolation of the most strongly

Table 6 A comparison between the lowest-energy dimers found for the triply-bonded $M'M''Cl_9^{3-}$ species

Parameter	M′M″						
	MoMo	MoW	WW	NbTc	NbRe	TaTc	TaRe
Electronic configuration	d^3d^3	$\sim d^{3.25}d^{2.75}$	d^3d^3	$\sim d^{1.5}d^{4.5}$	$\sim d^{1.8}d^{4.2}$	$\sim d^{1.5}d^{4.5}$	$\sim d^{1.7}d^{4.3}$
M′–Cl (terminal)/Å	2.46	2.48	2.46	2.50	2.49	2.49	2.49
M′–Cl (bridging)/Å	2.53	2.52	2.53	2.52	2.55	2.51	2.53
M′–M″ distance/Å	2.30	2.41	2.45	2.41	2.48	2.49	2.51
M″–Cl (bridging)/Å	2.53	2.49	2.53	2.51	2.51	2.53	2.53
M″–Cl (terminal)/Å	2.46	2.48	2.46	2.42	2.43	2.42	2.43
$D(M'Cl_6–M''Cl_3)^{3-}$/eV	6.26[a]	6.52[a]	6.77[a]	−1.47[c]	−0.67[c]	−1.67[c]	−0.78[c]
$D(M'Cl_3–M''Cl_6)^{3-}$/eV	6.26[b]	6.37[b]	6.77[b]	−0.37[d]	−0.62[d]	0.15[d]	−0.01[d]

Notes:[a] For dissociation to $M'Cl_6^{3-}$ and $M''Cl_3$. [b] Dissociation to $M'Cl_3$ and $M''Cl_6^{3-}$. [c] Dissociation to $M'Cl_6^{2-}$ and $M''Cl_3^{-}$. [d] Dissociation to $M'Cl_3^{-}$ and $M''Cl_6^{2-}$.

bonded mixed-group dimers. In this context also, we note that while the barriers to dissociation of the $M'MnCl_9^{3-}$ complexes are consistently below 0.5 eV, the corresponding barriers for scission of the multiply-bonded $M'M''Cl_9^{3-}$ (M′ = Nb, Ta; M″ = Tc, Re) dimers are all apparently higher than 2 eV according to our calculations. These calculated gas-phase barriers cannot reliably indicate a given dimer's stability, or lack thereof, within solution, but at the least they do suggest that fragmentation of the weakly-bridged $M'MnCl_9^{3-}$ dimers, whether unimolecular or under the influence of some ambient reagent, is more facile than the corresponding process for the 'triply bonded' dimers.

Conclusion

The structural diversity evident within the series of V/Mn mixed-group dimers, $M'M''Cl_9^{3-}$ is, according to our calculations, greater than that seen among analogous same-group dimers, with metal–metal separations ranging from 2.41 Å (in $NbTcCl_9^{3-}$, denoting an effective triple bond between metal atoms in a typical face-shared bioctahedral complex) to 4.22 Å (in $TaMnCl_9^{3-}$, which is essentially a $[TaCl_6^{2-}]\cdot[MnCl_3^{-}]$ dimer, with some edge-shared character, held together solely by van der Waals attraction). Notwithstanding the broad structural range seen, the polarization of the intermetallic axis (which is a consistent feature of all of these mixed-group dimers, and is evident to a varying degree on all of the broken-symmetry and associated state (S = 0, S = 2, and S = 3) potential energy surfaces) has a generally destabilising effect with respect to dimer fragmentation. This destabilizing effect, the preference for ferromagnetic coupling, and the magnitude of M′ ⟶ M″ electron transfer are all greatest when M′ (the V-group metal) is second- or third-row and M″ (the Mn-group metal) is manganese itself. In contrast, the extent of M′ ⟶ M″ electron transfer is least in the $VTcCl_9^{3-}$ and $VReCl_9^{3-}$ dimers, which each show a preference for antiferromagnetic coupling in a complex with intermetallic σ bonding but lacking significant additional (δ_π) metal–metal bonding character. The general tendency towards intermetallic electron transfer appears to be well modelled by a simple expression involving the spin polarization energy of each metal, and the ligand-field splitting of t_{2g} and e_g orbitals, in the corresponding d^3-valence hexachloro octahedral complex.

Acknowledgements

We gratefully acknowledge the Australian Research Council (ARC) for financial support.

References

1 F. A. Cotton and R. A. Walton, *Multiple Bonds between Metal Atoms*, Clarendon Press, Oxford, 1993.
2 G. J. Wessel and D. J. W. Ijdo, *Acta Crystallogr.*, 1957, **10**, 466.
3 A. Earnshaw and J. Lewis, *J. Chem. Soc.*, 1961, 396.
4 F. A. Cotton, *Rev. Pur. Appl. Chem.*, 1967, **17**, 25.
5 R. Saillant and R. A. D. Wentworth, *Inorg. Chem.*, 1968, **7**, 1606.
6 P. D. W. Boyd, P. W. Smith and A. G. Wedd, *Aust. J. Chem.*, 1969, **22**, 653.
7 I. E. Grey and P. W. Smith, *Aust. J. Chem.*, 1971, **24**, 73.
8 T. Ziegler and W. M. Risen, Jr., *Inorg. Chem.*, 1972, **11**, 2796.
9 D. V. Korol'kov and K. Missner, *Teor. Eksp. Khim.*, 1973, **9**, 336.
10 J. R. Beswick and D. E. Dugdale, *J. Phys. C*, 1973, **6**, 3326.
11 O. Kahn and B. Briat, *Chem. Phys. Lett.*, 1975, **32**, 376.
12 L. Dubicki and Y. Tanabe, *Mol. Phys.*, 1977, **34**, 1531.
13 K. R. Barry, K. J. Maxwell, K. A. Siddiqui and K. W. H. Stevens, *J. Phys. C*, 1981, **14**, 1281.
14 B. Leuenberger and H. U. Güdel, *Inorg. Chem.*, 1986, **25**, 181.
15 R. Stranger, A. Turner and C. D. Delfs, *Inorg. Chem.*, 2001, **40**, 4093.
16 M. S. Matson and R. A. D. Wentworth, *Inorg. Chem.*, 1976, **15**, 2139.
17 S. Petrie and R. Stranger, *Polyhedron*, 2002, **21**, 1163.
18 S. Petrie and R. Stranger, *Inorg. Chem.*, 2002, **41**, 2341.
19 S. Ferguson-Miller and G. T. Babcock, *Chem. Rev.*, 1996, **96**, 2889.
20 H. Michel, J. Behr, A. Harrenga and A. Kannt, *Annu. Rev. Biophys. Biomol. Struct.*, 1998, **27**, 329.
21 A. Volbeda, M.-H. Charon, C. Piras, E. C. Hatchikian, M. Frey and J. C. Fontecilla-Camps, *Nature*, 1995, **373**, 580.
22 G. Schenk, C. L. Boutchard, L. E. Carrington, C. J. Noble, B. Moubaraki, K. S. Murray, J. de Jersey, G. R. Hanson and S. Hamilton, *J. Biol. Chem.*, 2001, **276**, 19084.
23 A. Ceulemans, L. F. Chibotaru, G. A. Heylen, K. Pierloot and L. G. Vanquickenborne, *Chem. Rev.*, 2000, **100**, 787.
24 R. Stranger, J. E. McGrady and T. Lovell, *Inorg. Chem.*, 1998, **37**, 6795.
25 T. Lovell, R. Stranger and J. E. McGrady, *Inorg. Chem.*, 2001, **40**, 39.
26 E. J. Baerends, A. Bérces, C. Bo, P. M. Boerrigter, L. Cavallo, L. Deng, R. M. Dickson, D. E. Ellis, L. Fan, T. H. Fischer, C. Fonseca Guerra, S. J. A. van Gisbergen, J. A. Groeneveld, O. V. Gritsenko, F. E. Harris, P. van den Hoek, H. Jacobsen, G. van Kessel, F. Kootstra, E. van Lenthe, V. P. Osinga, P. H. T. Philipsen, D. Post, C. Pye, W. Ravenek, P. Ros, P. R. T. Schipper, G. Schreckenbach, J. G. Snijders, M. Sola, D. Swerhone, G. te Velde, P. Vernooijs, L. Versluis, O. Visser, E. van Wezenbeek, G. Wiesenekker, S. K. Wolff, T. K. Woo and T. Ziegler, *ADF2000*, 2000.
27 C. Fonseca Guerra, J. G. Snijders, G. te Velde and E. J. Baerends, *Theor. Chem. Acc.*, 1998, **99**, 391.
28 R. G. Parr and W. Yang, *Density Functional Theory of Atoms and Molecules*, Oxford University Press, London, 1989.
29 S. H. Vosko, L. Wilk and M. Nusair, *Can. J. Chem.*, 1980, **58**, 1200.
30 J. E. McGrady, R. Stranger and T. Lovell, *J. Phys. Chem. A*, 1997, **101**, 6265.
31 M. R. Bray, R. J. Deeth, V. J. Paget and P. D. Sheen, *Int. J. Quantum Chem.*, 1997, **61**, 85.
32 K. Besançon, G. Laurenczy, T. Lumini, R. Roulet and R. Bruyndonckx, *Inorg. Chem.*, 1998, **37**, 5634.
33 A. J. Bridgeman and G. Cavigliasso, *J. Phys. Chem. A*, 2001, **105**, 7111.
34 A. D. Becke, *J. Chem. Phys.*, 1992, **96**, 2155.
35 S. Petrie and R. Stranger, in preparation.
36 M. S. Matson and R. A. D. Wentworth, *J. Am. Chem. Soc.*, 1974, **96**, 7837.
37 L. Versluis and T. J. Ziegler, *J. Chem. Phys.*, 1988, **88**, 322.
38 J. E. McGrady, T. Lovell and R. Stranger, *Inorg. Chem.*, 1997, **36**, 3242.
39 L. Noodleman and J. G. Norman, Jr., *J. Chem. Phys.*, 1979, **70**, 4903.
40 T. Lovell, J. E. McGrady, R. Stranger and S. A. Macgregor, *Inorg. Chem.*, 1996, **35**, 3079.
41 J. E. McGrady, R. Stranger and T. Lovell, *Inorg. Chem.*, 1998, **37**, 3802.
42 S. Petrie and R. Stranger, *Inorg. Chem.*, 2002, in press.